Nano Today 49 (2023) 101760

Contents lists available at ScienceDirect

Nano Today

journal homepage: www.elsevier.com/locate/nanotoday

# Accordion-inspired parallelly assembled triboelectric nanogenerator: For efficient biomechanical energy harvesting and music responding

Linan Feng [a,b], Zhong Lin Wang [a,b,c,*], Xia Cao [b,d,e,f,g,*], Liqun Zhang [a,**]

[a] Beijing University of Chemical Technology, North Third Ring Road 15, Chaoyang District, Beijing 100029, China
[b] Beijing Institute of Nanoenergy and Nanosystems, Chinese Academy of Sciences, Beijing 101400, China
[c] School of Materials Science and Engineering, Georgia Institute of Technology, Atlanta, GA 30332-0245, United States
[d] Research Center for Bioengineering and Sensing Technology, Beijing Key Laboratory for Bioengineering and Sensing Technology, School of Chemistry and Biological Engineering, and Beijing Municipal Key Laboratory of New Energy Materials and Technologies, University of Science and Technology Beijing, Beijing 100083, China
[e] Research Centre of Information Technology, Shenzhen Institute of Information Technology, Shenzhen 518172, China
[f] Shenzhen Institute for Advanced Study, University of Electronic Science and Technology of China, Shenzhen 518000, China
[g] Center on Nanoenergy Research, School of Physical Science & Technology, Guangxi University, Nanning 530004, China

ARTICLE INFO

*Article history:*
Received 12 October 2022
Received in revised form 7 December 2022
Accepted 8 January 2023
Available online xxxx

*Keywords:*
Biomechanical energy
Parallel assembly
Triboelectric nanogenerator
Portable electronic devices

ABSTRACT

Harvesting biomechanical energy from human motion presents a promising supplement to electrochemical power sources such as batteries for portable electronic devices. In this paper, an array parallelly assembled triboelectric nanogenerator (PS-TENG) is proposed as an inspiration from the structure of accordion. The as-designed TENGs generate sustainable electrical power through hand motion with significantly enhanced electrification efficiency and reliability. The output of the parallelly assembled TENGs (PS-TENGs), which is positively correlated with the frequency of excitation and reciprocating distance, is 2.8 times higher than that of TENG with series electrodes(S-TENGs) under the same operating conditions. In addition, based on PS-TENGs can be used as self-powered sensors for smart home applications. Such a design promotes the application of TENG in powering portable electronic devices.



## Introduction

The Internet of Things (IoT) is reshaping the world and have the potential to reach every corner of our life. The ubiquitous IoT is now portable, wearable[1–3], and implantable[4,5], sensing[6] and in charging everything around us[7], and rapidly changing the way we live[8]. While revolutionizing out life for the better, great concern also is being expressed to the negative impact of e-waste on the environment that originates from the large-scale use of rechargeable batteries[9–11] as portable power sources[12–14]. With a limited cycle life, electrochemical batteries exert long-term effects of on soil, water, and air quality if the toxic materials are not fully recycled [3,15]. As a result, clean energies that can be harvested from human movement[2,16] or ambient environmental[6,17,18] are attracting considerable attention, as demonstrated by the fast development of energy converting technologies such as solar[19], thermoelectric [20–22] and electromagnetic nano-generators[13,23].

Recently, Wang et al.[9,24] invented TENG to convert mechanical energy into alternating current based on the coupled effects of frictional electrification and electrostatic induction during periodic contact and separation[25] via the following four modes: vertical contact-separation mode, lateral sliding mode, single electrode mode, and independent mode[9]. Currently, TENG has become a promising micro power source wits low cost, high yield and wide range of materials [7,24,26], which allows for the extraction of electrical energy from the abundant mechanical energy existing in the living environment, thus offering a wide variety of power sources for the development of IoTs.

Biomechanical energy[27,28] that can be harvested from human motion represents a promising clean alternative to electrical power supplied by electrochemical batteries for wearable or implanted electronic devices. However, biomechanical energy is difficult to efficiently utilize via the classical energy-harvesting technologies

* Corresponding authors at: Beijing Institute of Nanoenergy and Nanosystems, Chinese Academy of Sciences, Beijing 101400, China.
** Corresponding author.
*E-mail addresses:* zlwang@gatech.edu (Z.L. Wang), caoxia@binn.cas.cn (X. Cao), zhanglq@mail.buct.edu.cn (L. Zhang).

https://doi.org/10.1016/j.nantod.2023.101760
1748-0132/

due to the fluctuating amplitudes and variable low frequency. To promote the efficiency of biomechanical energy harvesting, many investigations have been devoted to material selection[10,15], structure and mechanical design[6,14,19,23], and surface engineering[14,29]. Nevertheless, the large electrode resistance of the device remains a critical issue[30], which hinders the rising of the output power and restricts its practical application in self-powered systems.

To solve the above-mentioned problem, we may start from the basic physical concept of small resistance in parallel circuits. When the matched external resistance ($R_e$) is in balance with the internal resistance ($R_f$), the instantaneous power density (W) is at its peak for a specific power supply with a constant output voltage (V). On the basis of

$$W = I^2R_e = \left(\frac{V}{R_e + R_f}\right)R_e = \frac{V^2}{2R_f + R_e + R_f^2/R_e} \quad (1)$$

It can be seen that in a typical TENG, $R_f$ is of great significance as regards the output performance, and in some case a very high resistance dramatically impairs the output performance of the triboelectric nanogenerator. Meanwhile, if an electrode of resistance R is made into N, the resistance of an individual electrode is R/N, and the resistance $R_A$ can be expressed as $R_A$=R/$N^2$ if these individual electrodes are connected in parallel. Consequently, switching from a series circuit to a parallel circuit would dramatically diminish the resistance of the circuit and the output current of TENG would be thus enhanced if it is connected in parallel using multiple single electrodes[30].

Thus, in this paper, TENGs inspired by the unique arrangement of accordions and Oreo sandwich are proposed for biomechanical energy harvesting. The output of PS-TENG and S-TENG are systematically compared under different stimulations. The results show that the PS-TENG enhances the output electrical signal to 350 V, 35.1 μA, which is 2.8 times higher than that of the S-TENG. At the same time, the dependence of the electrical output on the number of triboelectric cells and the material of the dielectric layer is measured, and the relationship between reciprocating distance, excitation frequency and the output of PS-TENG is also experimentally investigated. In addition, it takes only 66 s to bring 100 μF@ 25–40 V, effectively powers 204 LEDs, and lights potable electronics such as watch, calculator, hygrometer and the music component, proving the PS-TENG's potential for harvesting biomechanical energy from human motion.

## Results and discussion

Fig. 1a(i) shows the schematic structure of an accordion, and the interior consists of several parallel reeds. When stretching in a reciprocating motion, the paralleling of the reeds enables every cell to move the same distance. Fig. 1a(ii) exhibits the Oreo sandwich structure. Through the simulation of the distinctive arranging of accordion and Oreo sandwich, based on which a TENG consisting of several triboelectric units is proposed, as shown in Fig. 1a(iii).

Fig. 1b depicts the assemble process of the as-designed TNEG, where a single frictional cell consists of two different frictional layers and two additional electrodes. The negative friction layer is divided into two layers, a conductive layer (yellow) made of Ag electrodes on the left and a friction layer (purple) made of a sheared circular PVC film on the right, with a genus wire attached to the edge of the Al surface using a double layer of conductive aluminum tape. And for the positive friction layer part, another wired PA (blue) /Al electrode is used, where frictional electricity generation occurs between the PVC surface and the PA surface.

In order to describe the electrical output of the as-designed TNEG (PS-TENG, S-TENG), a single triboelectric cell operating in a tensile reciprocating motion is designed to collect energy (Fig. 1c). Two electrodes are connected to an ammeter. In the original state, the device remains neutral under the absence of any external force. When an external force is imposed, there is a contact between the PVC and the PA surface, electrons will be injected from the PA film to the surface of PVC film, thus leading to a positive charge on the PA film and a negative charge on the PVC film. As the force is removed, these two layers will separate from each other. Due to the electrostatic effect, the electrostatic charge remaining on the surface creates a potential difference between the two electrodes, resulting in a flow of free-charge to generate a current signal. Once the layers are completely separated, a new equalization is reached between each layer and the attached electrodes. As soon as the force is re-applied and the PVC film comes into contact with the PA film again, the electrons flow back in reverse to balance the charge and generate a reverse output. In Fig. 1d, a theoretical investigation of the as-designed TNEG during the stretching process is conducted. COMSOL Multiphysics simulation data reveal the potential distribution among the top and bottom electrodes with different gaps.

In accordance with the triboelectric electric order of the materials, the output performance of TENG is different in case of different triboelectric electric materials. Here, the open-circuit voltage (Fig. 1e) and short-circuit current (Fig. 1 f) obtained for the nylon material with six other typical materials, including metal (aluminum foil) and polymer (Polyimide (PI), Polytetrafluoroethylene (PTFE), polyethylene terephthalate (PET), Fluorinated ethylene propylene (FEP), Polyvinyl chloride (PVC)) at the same frequency as well as the same contact area were examined. It can be noted that the output performance of PVC film as a friction layer is much more superior compared to other triboelectric materials, as shown in Fig. 1 g.

Fig. 2a is the photograph of the original PS-TENG, and the inset is the detail picture of PS-TENG. To compare effect of series and parallel connection on the electrical output of the as-designed TNEG, the voltage (Fig. 2b), current (Fig. 2c), and transferred charge (Fig. 2d) of the S-TENG, PS-TENG composed of two triboelectric cells under different excitation conditions (frequency, reciprocal distance) were measured. From a general point of view, the frequency of excitation is a positive correlation with the electrical output. Nevertheless, it is apparent that the output performance of the PS-TENG is consistently superior to that of the S-TENG under the same conditions (Fig. 2b-d).

Fig. (2e-f) give a detailed comparison of the open-circuit voltage and short-circuit current of a PS-TENG containing different numbers of triboelectric cells at 3 Hz. It is very intuitive to visualize that both voltage and current rise with a growing number of friction cells when the frequency is a constant. Therefore, a TENG with 10 triboelectric cells is considered as the subject of the experiment.

As illustrated in Fig.(3a-c), it is shown that the increase of the reciprocal distance results in the enhancement of the voltage, current and transferred charge. For the high frequency excitation with reciprocal distance from 11 cm to 15–19 cm, the peak-to-peak voltage, current, and transferred charge of PS-TENG are 314–336–350 V, 20–25.4–35.1μA, and 300–354–375 nC, respectively, which are greatly exceeded by the output of S-TENG: 82–90–122 V, 8–9.3–12.8 μA, 29–31–39.65 nC. In addition, the two TENGs' peak-to-peak outputs are compared for different frequencies. In this process, under the excitation of the repetitive distance of 19 cm, with the increasing

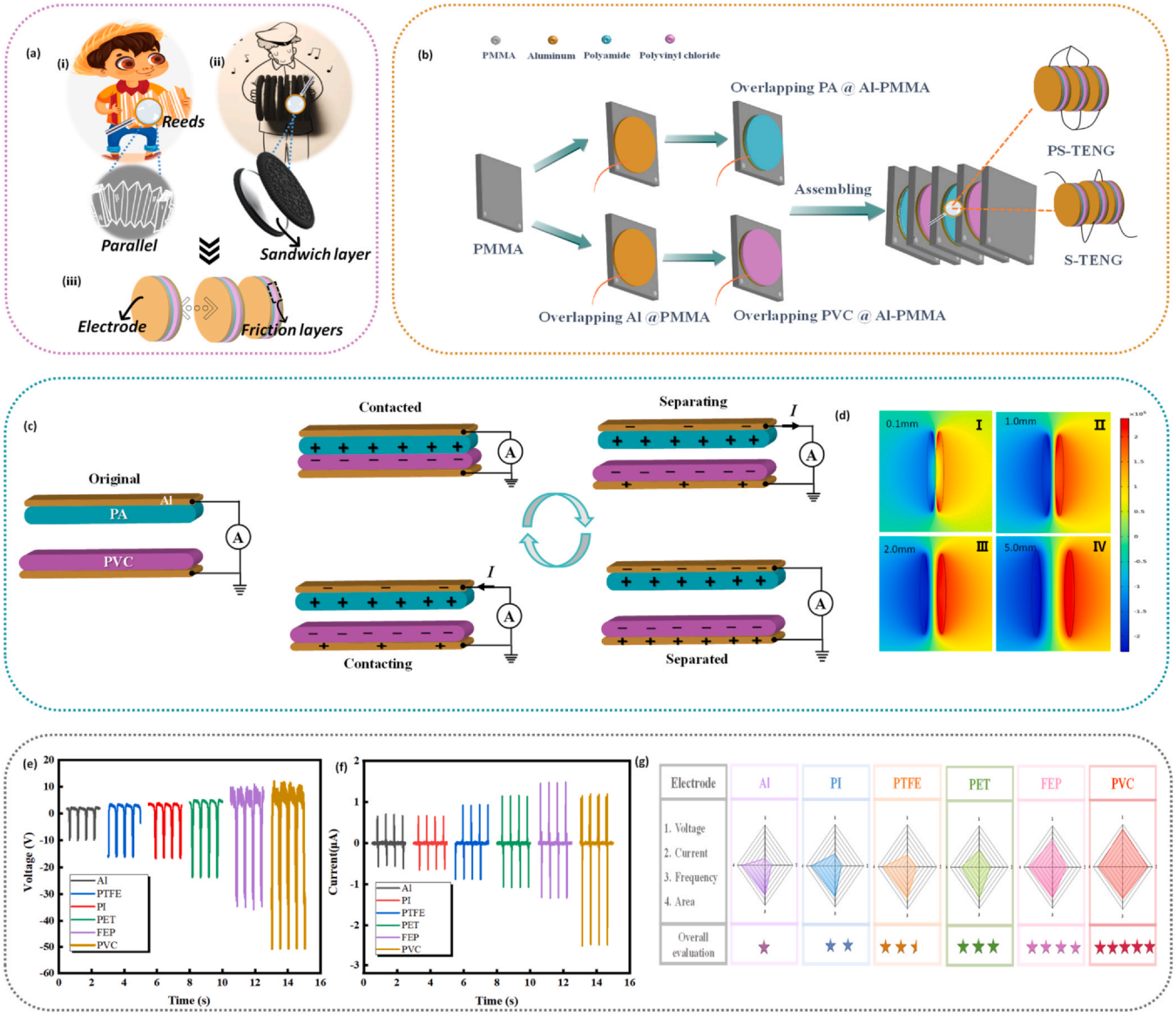


**Fig. 1.** (a) Accordion samples (b) The preparation process of TENG; (c) Working mechanism of the as-designed PS-TENG; (d) Simulated potential distribution with different spacing between electrodes. Comparison of the open-circuit voltage (e) and short-circuit current (f) of TENG using different material; (g) Comparative diagram on the performance of the advantages and disadvantages among the various friction materials.

frequency, the peak voltage of PS-TENG grows from 319 V to 350 V and S-TENG rises from 93 V to 122 V (Fig. 3a), the peak-to-peak current of PS-TENG grows from 20.75 μA to 35.1 μA and S-TENG goes up from 9.2 μA to 12.8 μA (Fig. 3b), and the peak-to-peak current of PS-TENG grows from 338 nC to 375 nC and S-TENG goes up from 32 nC to 39.65 nC (Fig. 3c). It has been reported by researchers that the increase in electrical output depending on frequency is owing to the build-up of triboelectric charges[31]. In a cycle, as the frequency increased, a larger number of charges are generated and at the meantime the shortened neutralization time of the charges between the two materials, which causes some charges not to be completely neutralized in an excitation cycle and thus accumulated on the surface of the triboelectric electric material. The results reveal that the increasing reciprocal distance and frequency lead to an increase in the electrical output of both PS-TENG and S-TENG, but the output of PS-TENG always outperforms S-TENG under the same incentive conditions. This is in line with our previous discussion that parallel connection among electrodes leads to enhanced output performance of TENG compared to series connection by electrodes. Further, the performance of PS-TENG under a range of excitation conditions is highlighted.

The triboelectric layer was stretched to different positions of the spindle (Figure S2d-f) to investigate the effect of different reciprocating distances on the electrical output. The magnitude of the electrical signal changes along with the change of the position of the lower triboelectric layer while the excitation frequency of the PS-TENG is constant. The output voltage (Fig. 3d), current (Fig. 3e), and transferred charge (Fig. 3 f) increases when the position of the

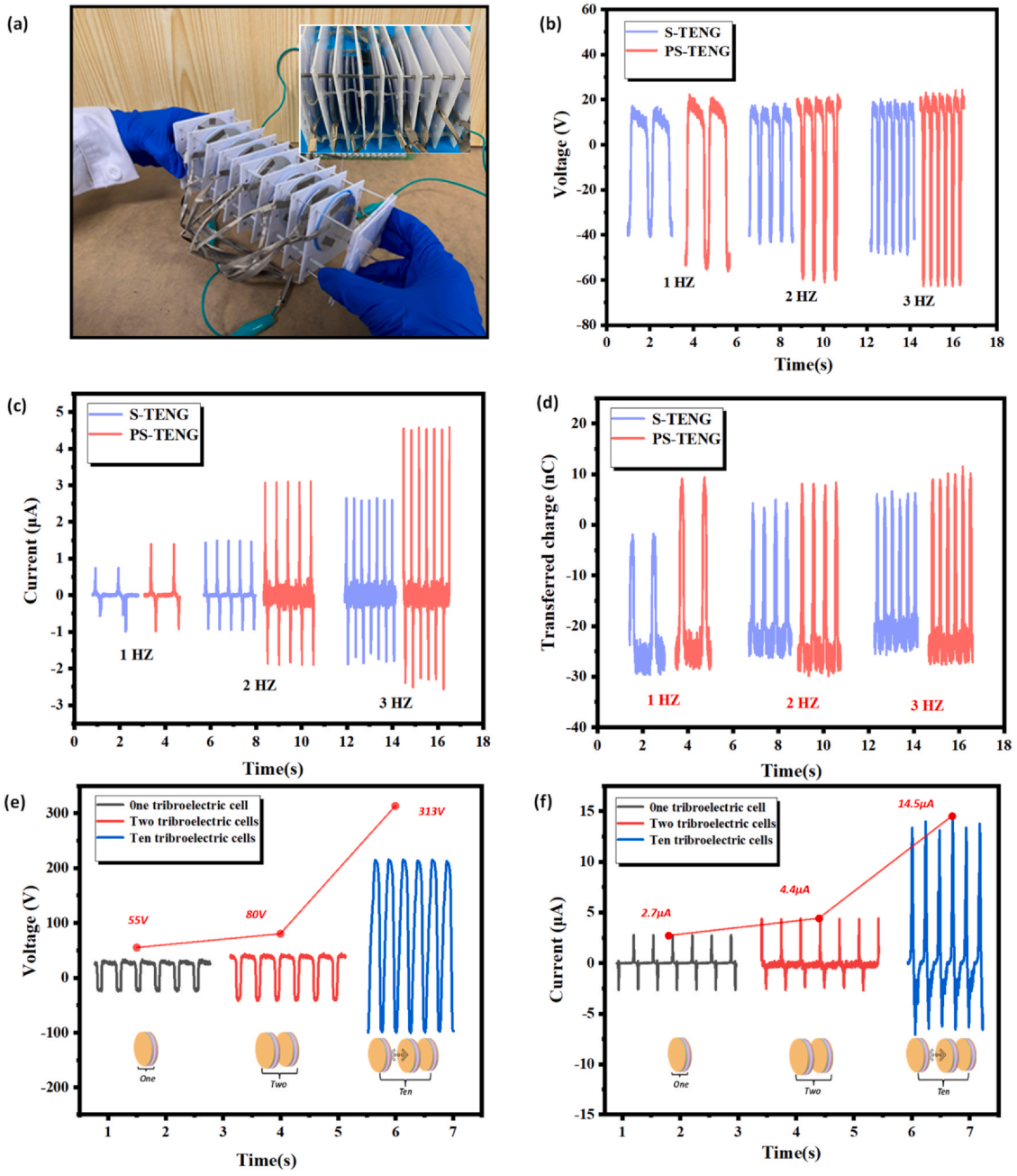


**Fig. 2.** The physical photo of PS-TENG(a). Output performance of two triboelectric cells with TENG at different frequencies (1 Hz, 2 Hz, 3 Hz) and connections (series, parallel connection): (b-d) voltage, current, transferred charge, (e-f) Effect of the number of triboelectric units on the open circuit voltage and short circuit current.

triboelectric layer changes from the 11 cm position to the 19 cm position at the same frequency. For example, under high-frequency excitation, the reciprocating distance increases from 11 to 19 cm, the voltage of 314 V goes up to 350 V, the current of 20 μA goes up to 35.1 μA, and the amount of transferred charge goes up from 0.300 μF to 0.3375 μF. Thus, this proves that the electrical signal output can be remarkably enhanced by increasing the reciprocating distance under the design of an accordion-initiated PS-TENG. According to Gauss' theorem, the voltage and charge generated by the PS-TENG can be expressed as:

$$V = -\frac{Q}{S\varepsilon_0}\left(\frac{d}{\varepsilon} + x\right) + \frac{\sigma x}{\varepsilon_0} \tag{2}$$

$$Q = \frac{S\sigma x}{d + x} \tag{3}$$

In the equation, x is the separation distance between two triboelectric electric layers, σ is the static charge density. $\varepsilon_0$ is the dielectric constant of the vacuum. d, ε, and S are the thickness, relative dielectric constant, and surface area, respectively. It can be easily

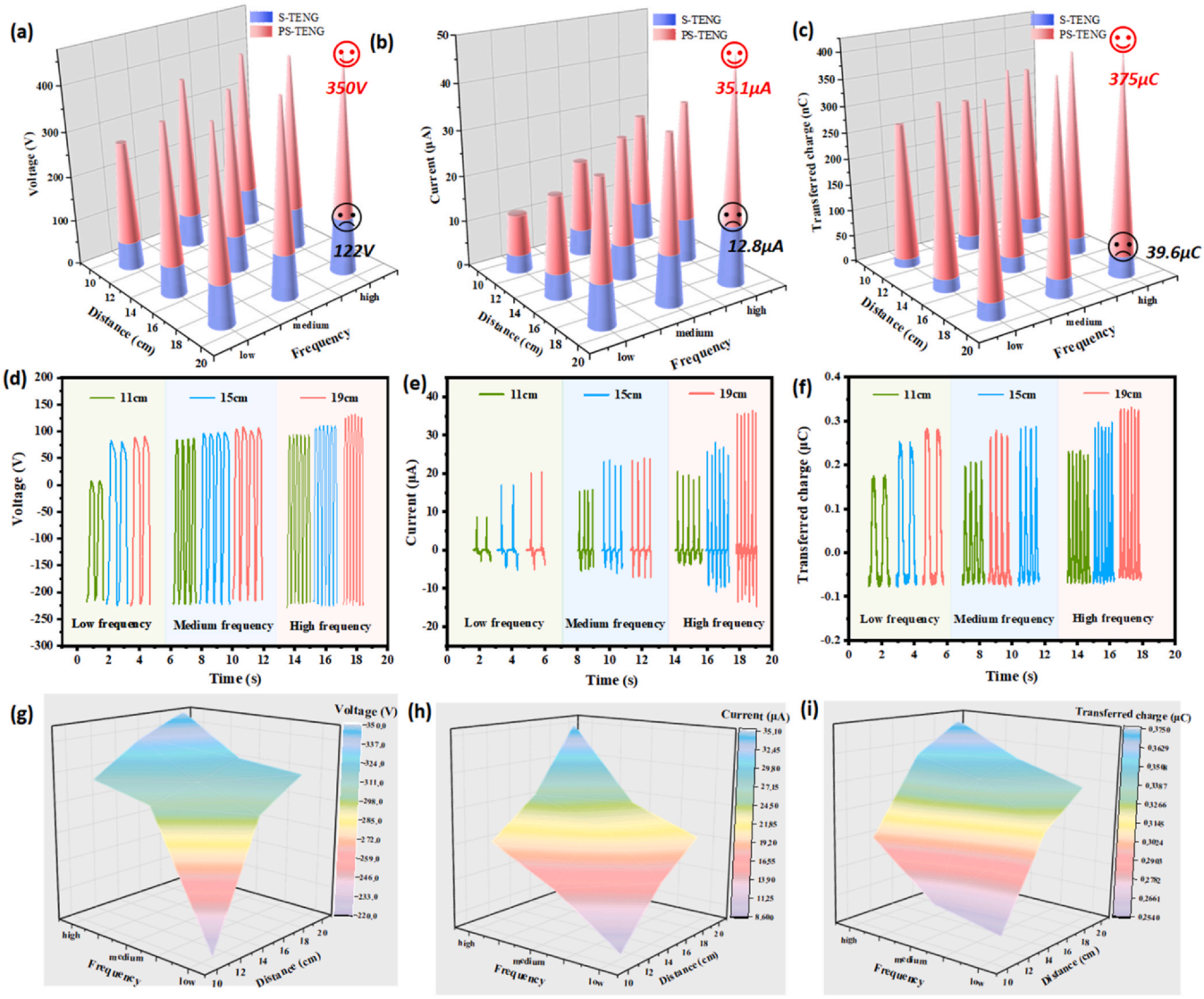


**Fig. 3.** Performance comparison of PS-TENG and S-TENG based on different excitation frequencies and reciprocating distances: (a) voltage, (b) current, (c) transferred charge. (d-f) Electrical output performance of PS-TENG at various excitation frequencies and reciprocating distances; RGB color diagram of PS-TENG output voltage (g), current (h), transferred charge (i) versus based on the frequencies and distances.

deduced from formula (2) and (3) that once the material properties and contact area are determined, the voltage and the amount of transferred charge are only related to the distance x, so the output voltage and transferred charge increases continuously with the separation distance, which is in accordance with the reported references[30,31].

During the position measurement of the triboelectric layer, the excitation frequency is adjusted to ensure that the maximum electrical output occurred. At the same time, assuming that in one cycle of the triboelectric process, the charge transfer between the two triboelectric layers is fixed as Q, the corresponding current can be defined as: I=Q/t. It is of no surprise that the intensity of the current is inversely proportional to the time interval of the charge change, i.e., as the frequency increased, the shorter the contact time of one cycle, its intensity would be enlarged. For example, in Fig. 3e, it can be observed that under the condition of the same reciprocal distance, the current grows when switching from low to high frequency (e.g., when the reciprocal distance is fixed at 19 cm, the current to 35.1 μA increases from 20.7). Based on the data and theoretical analysis, it can be summarized that the stretching frequency affects the amplitude of the current rather than the amplitude output of the interfering signal. It is proved that the PS-TENG can work reliably at various frequencies. Fig. (3 g, h, i) illustrate the integrated effect of excitation frequency and reciprocation distance on the PS-TENG output, as reflected by the calmness of the surface: the output electrical signal becomes larger as the stronger excitation frequency and the larger reciprocation distance.

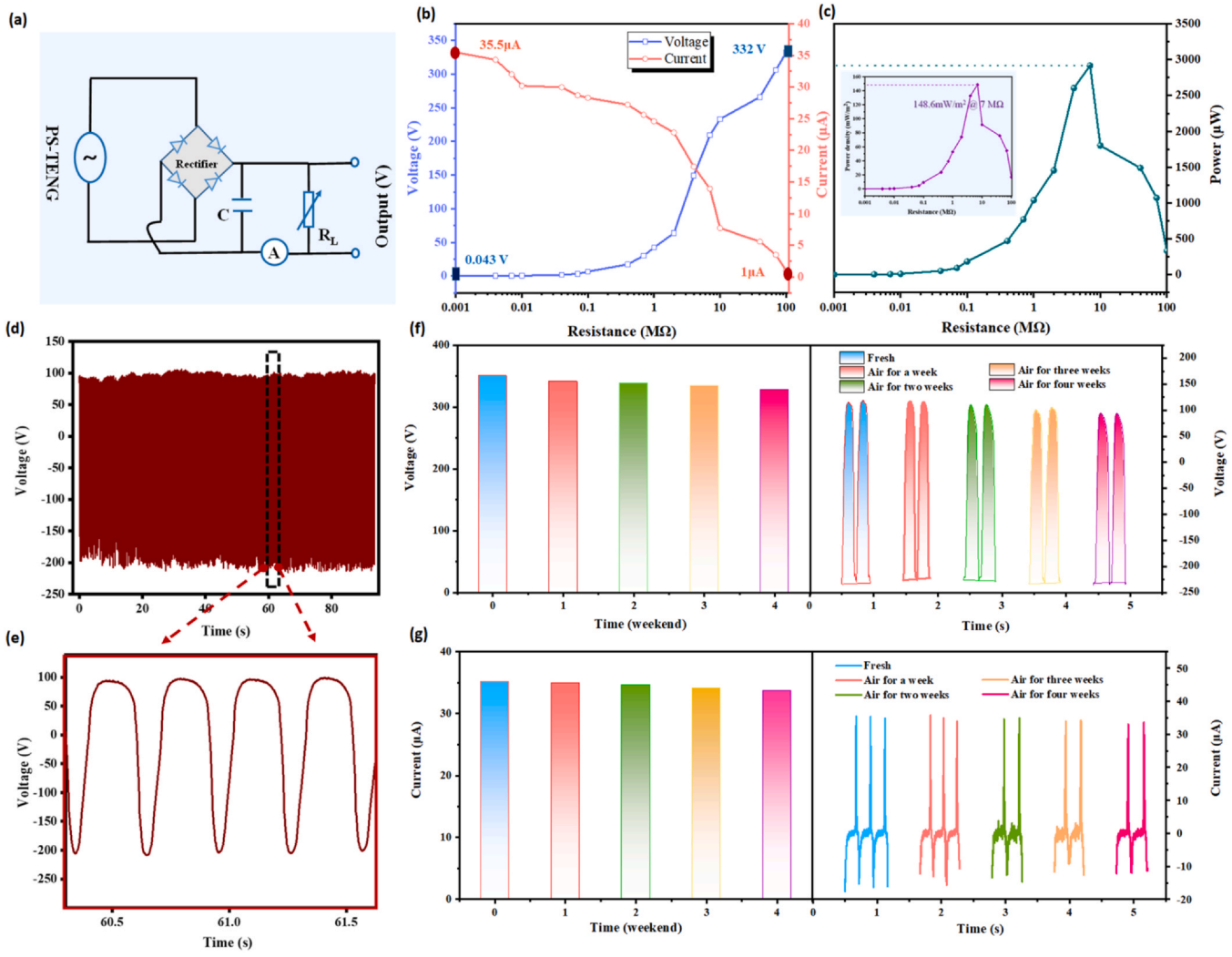


**Fig. 4.** (a) Load resistance after rectification with output circuit diagram. The load resistance dependence of (b) output voltage, output current, (c) output power of PS-TENG. (d-e) The circulation experiment of PS-TENG. (f-g) The environmental stability analysis of PS-TENG.

Since the matching of impedance and output power is an important method to obtain excellent performance, we have further investigated the power at different resistances to improve the output performance of PS-TENG. The experiments are all performed at a high frequency-distance of 19 cm excitation. The PS-TENG is connected to the rectifier bridge, forming a circuit diagram as shown in Fig. 4a. By a gradually increasing external resistance, the voltage signal gradually grows up as well as the current gradually drops. when the load resistance increases from 0.001 MΩ to 100 MΩ, the peak voltage of PS-TENG improves from 0.043 V to 332 V (Fig. 4b) and the peak current drops from 35.5 uA to 1.0 uA (Fig. 4b). It eventually leads to a first growth and then a decrease of the output power, then we can observe in Fig. 4c that at a matched impedance of 7 MΩ, the optimized output power and power density stands at 2916 μW,148.6 mW/m$^2$ respectively. We illustrate the durability of the PS-TENG by testing its continuous output. Fig. 4d shows the corresponding test results, and it can be seen that the PS-TENG is capable of consistent output, and Fig. 4e shows the partial enlarged diagram of the stable output. The performance reveals that a relatively stable electrical signal output is obtained after several repetitions, which also reveals the comparatively high stability of our device. As shown in Fig. 4f-g, the electrical output of PS-TENG can be tested after four weeks of storage in air to characterize the environmental stability of PS-TENG.

The performance of the PS-TENG is further investigated by charging capacitors for 200 s under high frequency – 19 cm excitation, shown in the inset of Fig. 5b. A rectifier is introduced into the circuit to convert the alternation current into direct current. Five capacitors of 3.3 μF, 4.7 μF, 10 μF, 47 μF and 100 μF with rated voltage of 25 V were adopted as accumulators, and their charging curves all indicate a constant increase in capacitor voltage when the PS-TENG performs a reciprocal tapping motion (Fig. 5b). For capacitors of 3.3 μF, 4.7 μF, 10 μF, 47 μF, and 100 μF, the charging voltages can be as high as 3.3 V, 12 V, 40 V, 63 V, and 75 V at 200 s, respectively (Fig. 5b). The charging rates of different capacitors are calculated to be 0.6 V/s @ 3.3 μF, 0.49 V/s @ 4.7 μF, and 0.2 V/s @ 10 μF, respectively, when

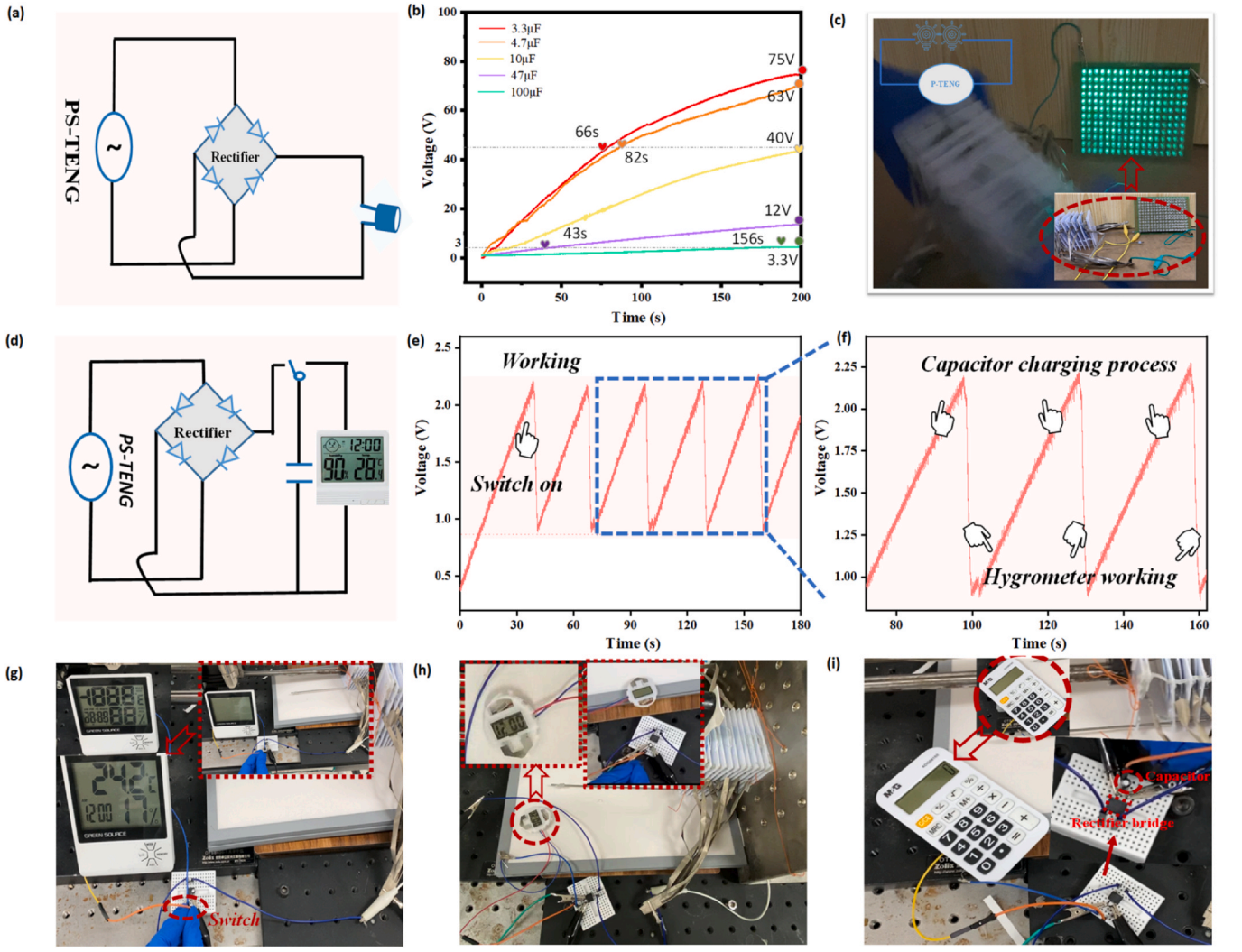


**Fig. 5.** (a) Charging circuit diagram after rectification. (b) Voltage comparison curves of PS-TENG charging 3.3 μF, 4.7 μF, 10 μF, 47 μF, and 100 μF capacitors respectively. (c) Circuit for lighting 204 green leds and PS-TENG image of illuminated led. (d) PS-TENG circuit diagram with power supply for hygrometer, (e) Voltage-time curve of the hygrometer. (f) Detailed voltage profile of the selected area in (e). (g) Image of PS-TENG successfully powering a hygrometer. Photos of PS-TENG successfully lighting up the (h) watch, (i) calculator.

the voltage reached to 40 V. The above findings demonstrate the high charging rate of the PS-TENG. This power can be further used to drive electronic devices by using the storage of the capacitor. Then, we have designed the circuit to light up the LEDs (Fig. 5c) and have experimented with the performance of the PS-TENG to supply power to the LED array (supporting information video S1–2). Connecting the PS-TENG directly to 204 green light-emitting diodes (LEDs), the high output generated by the periodic reciprocal motion lights up 204 small lights of good brightness.

Utilizing the collected power of the capacitor to drive the hygrometer, and its circuit diagram is shown in Fig. 5d. At first, the capacitor is charged by the PS-TENG, and once the voltage of the capacitor achieves 2.18 V (Fig. 5e), it switches to a functioning circuit connecting the capacitor and the hygrometer, at which time the screen of the hygrometer lights up, signifying a successful powering up of the hygrometer (supporting information video S3). In approximately 3 s or so, an amount of power is exhausted from the capacitor and by the time the voltage drops to about 0.88 V, there is not enough power to run the watch. Afterwards it is switched back to the circuit that charges the capacitor. As soon as the capacitor voltage re-attains 2.18 V, the screen of the hygrometer lights up again, presenting a repeated cyclic process (Fig. 5e-f). Fig. 5 g is the real photograph. Immediately after, the charging capacitor successfully powers the watch and calculator, proving once again the charging performance and further displaying the commercial potential of the PS-TENG, Fig. (5h-i) present photos of the scene.

Amazingly, the PS-TENGs can be used not only to stretch the exercise arms, but also as a switch to control the music device (Fig. 6b). When we stretch the device to exercise our body, the PS-TENGs will send a signal to make the music element respond (Fig. 6c-d), thus playing beautiful music, and we can stretch to exercise arm strength while listening to beautiful music (Fig. 6e). Once we stop exercising, the PS-TENGs have no output to respond to the music element, and thus the song is turned off. Such intelligent PS-

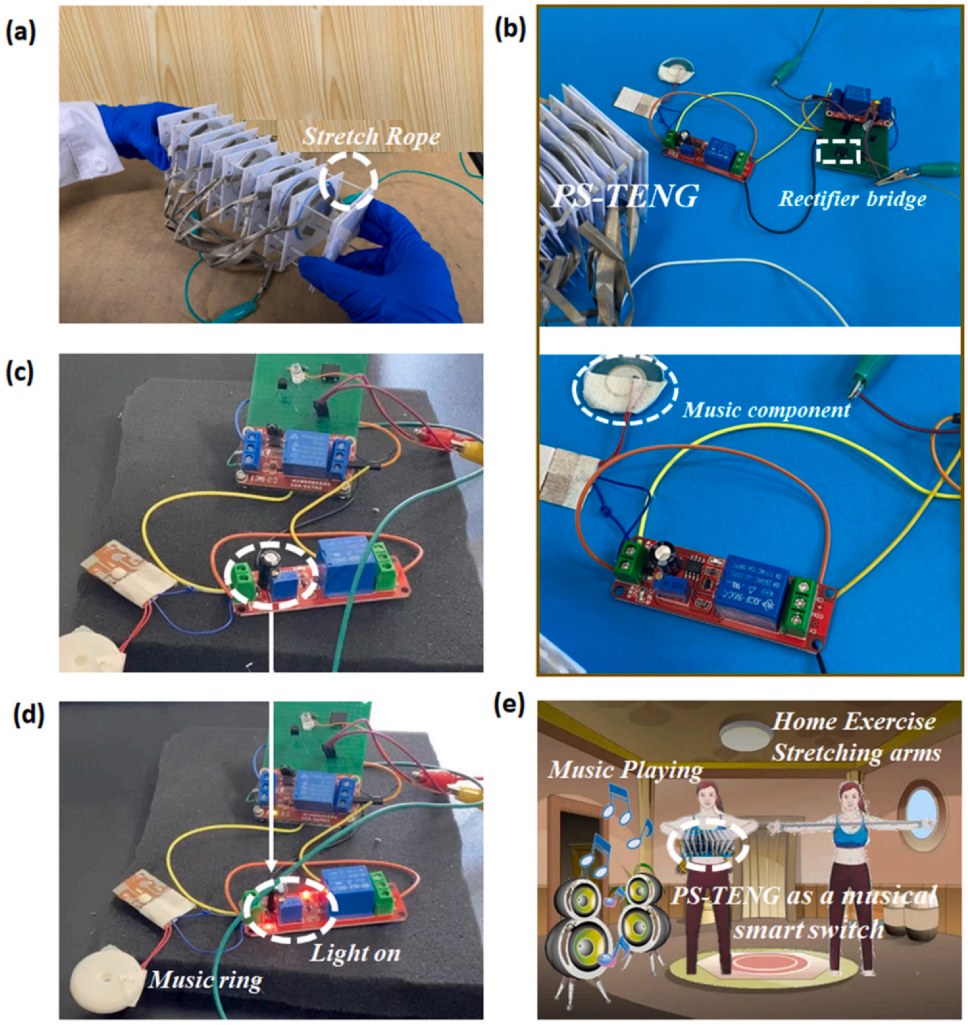


**Fig. 6.** The physical photo of PS-TENG(a); (b) Experimental diagram of the PS-TENG -driven musical switch. (c-d) PS-TENG switch to control music component; (e) Stretch the PS-TENG at home to exercise arm strength and intelligently control the music switch.

TENGs we designed to control the music switch device is very intelligent, but also to develop children's hands-on skills, educational and fun. For more detailed information, see the supporting information in video S4, video S5 and video S6.

## Conclusion

In this work, inspired by accordion and Oreo sandwich, PS-TENGs are proposed for efficient biomechanical energy harvesting. The power of the PS-TENGs can reach approximately 2916 μW when the load resistance is 7 MΩ, which is about 2.8 times higher than that of S-TENGs and can illuminate up to 204 LEDs and a range of electronic devices. Thus, we are making an exciting step toward bioenergy harvesting for self-powered electronics.

## Experimental section

*Design of multi-electrode parallel (PS-TENG) and multi-electrode series (S-TENG) structures*

As shown in Figure S2a, the positive triboelectric material (PA) is a circle with a diameter of 5 cm, and the negative triboelectric material (PVC) and silver electrode (Ag) have the same dimensions as those of PA. In addition, an acrylic plate is used as a support layer for the triboelectric layer with dimensions of 6 cm × 6 cm × 1 mm, on the two sides of each acrylic sheet, make five holes of 2 mm in diameter., as shown in Figure S2a. Subsequently, a rubber band is used to pass through the hole at the top, and after ensuring that the separation distance between the two triboelectric layers is fixed at 5 mm, each acrylic plate is fixed with the rubber band attached to it, as shown in Figure S2b. A hard wire with a diameter of 1.8 mm is passed through the hole at the bottom of the acrylic plate (Figure S2c), respectively, and the two ends of the iron rod are fixed with hot melt glue, and the distance between the two ends of the hot melt glue is 11 cm, 15 cm, and 19 cm, respectively, as shown in Figure (S2d-f). In the unstretched original state, the length of PS-TENG is about 11 cm,

including 10 triboelectric units, as shown in Figure S3a. In addition, S-TENG is also composed of 10 triboelectric units, as shown in Figure S3b.

*Electrical Output Measurements*

The electrical outputs of the PS-TENG and S-TENG were collected by potentiometers (Keithley 6514 system). The ZX21 rotary DC resistor box system is used to provide an external load in order to measure the power output of the PS-TENG.

## Author Contributions

This manuscript was written through contributions of all authors. All authors have given approval to the final version of the manuscript.

## Data Availability

Data will be made available on request.

## Declaration of Competing Interest

The authors declare that they have no known competing financial interests or personal relationships that could have appeared to influence the work reported in this paper.

## Acknowledgements

This work was financially supported by the National Key R & D Project from Minister of Science and Technology (2021YFA1201601), and the Key Research Program of Frontier Sciences, CAS (ZDBS-LY-DQC025). Patents have been filed to protect the reported inventions.

## Notes

The authors declare no competing financial interest.

## Appendix A. Supporting information

Supplementary data associated with this article can be found in the online version at doi:10.1016/j.nantod.2023.101760.

## References

[1] S. Li, J. Wang, W. Peng, et al., Sustainable energy source for wearable electronics based on multilayer elastomeric triboelectric nanogenerators, Adv. Energy Mater. 7 (13) (2017) 1602832.
[2] C. Hou, J. Geng, Z. Yang, et al., A delta-parallel-inspired human machine interface by using self-powered triboelectric nanogenerator toward 3D and VR/AR manipulations, Adv. Mater. Technol. 6 (1) (2020) 2000912.
[3] Y. Wu, Y. Luo, T.J. Cuthbert, et al., Hydrogels as soft ionic conductors in flexible and wearable triboelectric nanogenerators, Adv. Sci. 9 (11) (2022) e2106008.
[4] Q. Lu, H. Chen, Y. Zeng, et al., Intelligent facemask based on triboelectric nanogenerator for respiratory monitoring, Nano Energy 91 (2022) 106612.
[5] W. He, S. Li, P. Bai, et al., Multifunctional triboelectric nanogenerator based on flexible and self-healing sandwich structural film, Nano Energy 96 (2022) 107109.
[6] X. Xiao, X. Zhang, S. Wang, et al., Honeycomb structure inspired triboelectric nanogenerator for highly effective vibration energy harvesting and self-powered engine condition monitoring, Adv. Energy Mater. 9 (40) (2019) 1902460.
[7] X. Shi, J. Luo, J. Luo, et al., Flexible wood-based triboelectric self-powered smart home system, ACS Nano 16 (2) (2022) 3341–3350.
[8] X. Cao, Y. Jie, P. Ma, et al., Wherever there is a dynamic touch, there is electromagnetic field-a discovery for power generation, Nano Energy 78 (2020) 105314.
[9] Y. Liu, W. Yan, J. Han, et al., Aerodynamics-based triboelectric nanogenerator for enhancing multi-operating robustness via mode automatic switching, Adv. Funct. Mater. (2022) 2202964.
[10] G. Khandelwal, N.P. Maria Joseph Raj, S.J. Kim, Materials beyond conventional triboelectric series for fabrication and applications of triboelectric nanogenerators, Adv. Energy Mater. 11 (33) (2021) 2101170.
[11] X. Cao, Y. Jie, P. Ma, Power generation by contact and the potential applications in new energy[J], Nano Energy 87 (2021) 106167.
[12] J. Jiao, Q. Lu, Z. Wang, et al., Sandwich as a triboelectric nanogenerator, Nano Energy 79 (2021) 105411.
[13] X. Wang, Z.L. Wang, Y. Yang, Hybridized nanogenerator for simultaneously scavenging mechanical and thermal energies by electromagnetic-triboelectric-thermoelectric effects, Nano Energy 26 (2016) 164–171.
[14] M. Zhang, W. Zhu, T. Zhang, et al., Lever-inspired triboelectric nanogenerator with ultra-high output for pulse monitoring, Nano Energy 97 (2022) 107159.
[15] V.T. Bui, Q. Zhou, J.N. Kim, et al., Treefrog toe pad-inspired micropatterning for high-power triboelectric nanogenerator, Adv. Funct. Mater. 29 (28) (2019) 1901638.
[16] Y. Cao, Y. Yang, X. Qu, et al., A self-powered triboelectric hybrid coder for human-machine interaction, Small Methods 6 (3) (2022) e2101529.
[17] Z. Zhao, Z. Zhang, L. Xu, et al., Tumbler-shaped hybrid triboelectric nanogenerators for amphibious self-powered environmental monitoring, Nano Energy 76 (2020) 104960.
[18] J. Xue, N. Zheng, W. Zhao, et al., Rubik-cube-based self-powered sensors and system: an approach toward smart toys, Adv. Funct. Mater. 32 (1) (2021) 2107099.
[19] W. Du, X. Han, L. Lin, et al., A three dimensional multi-layered sliding triboelectric nanogenerator, Adv. Energy Mater. 4 (11) (2014) 1301592.
[20] W. Wu, X. Cao, J. Zou, et al., Triboelectric nanogenerator boosts smart green tires, Adv. Funct. Mater. 29 (41) (2018) 1806331.
[21] C. Liu, D.-L. Shan, Z.-H. Shen, et al., Role of interfaces in organic–inorganic flexible thermoelectrics, Nano Energy 89 (2021) 106380.
[22] X. Chen, L. Feng, P. Yu, et al., Flexible thermoelectric films based on Bi2Te3 nanosheets and carbon nanotube network with high n-type performance, ACS Appl. Mater. Interfaces 13 (4) (2021) 5451–5459.
[23] D. Lee, D. Kim, Dual output from unitary input for a hybrid coaxial triboelectric nanogenerator inspired by a crank engine, Nano Energy 71 (2020) 104599.
[24] B. Chen, Z.L. Wang, Toward a new era of sustainable energy: advanced triboelectric nanogenerator for harvesting high entropy energy, Small (2022) e2107034.
[25] W. Li, Y. Zhang, L. Liu, et al., A high energy output nanogenerator based on reduced graphene oxide, Nanoscale 7 (43) (2015) 18147–18151.
[26] L. Long, W. Liu, Z. Wang, et al., High performance floating self-excited sliding triboelectric nanogenerator for micro mechanical energy harvesting, Nat. Commun. 12 (1) (2021) 4689.
[27] J. Wang, Z. Jiang, W. Sun, et al., Yoyo-ball inspired triboelectric nanogenerators for harvesting biomechanical energy, Appl. Energy 308 (2022) 118322.
[28] D. Heo, J. Chung, G. Shin, et al., Yo-Yo inspired triboelectric nanogenerator, Energies 14 (7) (2021) 1798.
[29] G. Xu, D. Guan, J. Fu, et al., Density of surface states: another key contributing factor in triboelectric charge generation, ACS Appl. Mater. Interfaces 14 (4) (2022) 5355–5362.
[30] T. Jing, B. Xu, J.H. Xin, et al., Series to parallel structure of electrode fiber: an effective method to remarkably reduce inner resistance of triboelectric nanogenerator textiles, J. Mater. Chem. A 9 (20) (2021) 12331–12339.
[31] P. Yin, K.C. Aw, X. Jiang, et al., Fish gills inspired parallel-cell triboelectric nanogenerator, Nano Energy 95 (2022) 106976.

**Linan Feng** is currently a doctoral student jointly trained by Beijing University of Chemical Technology (BUCT) and Beijing Institute of Nanoenergy and Nanosystems, Chinese Academy of Sciences. Her research interests include frictional electric nanogenerators, self-powered micro/nanosystems, and energy materials.

**Zhong Lin** Wang received his Ph.D. from Arizona State University in physics. He now is the Hightower Chair in Materials Science and Engineering, Regents' Professor, Engineering Distinguished Professor and Director, Center for Nanostructure Characterization, at Georgia Tech. Prof. Wang has made original and innovative contributions to the synthesis, discovery, characterization and understanding of fundamental physical properties of oxide nanobelts and nanowires, as well as applications of nanowires in energy sciences, electronics, optoelectronics and biological science. His discovery and breakthroughs in developing nanogenerators established the principle and technological roadmap for harvesting mechanical energy from the environment and biological systems for powering personal electronics. His research on self-powered nanosystems has inspired the worldwide effort in academia and industry for studying energy for micro-nano-systems, which is now a distinct disciplinary in energy research and future sensor networks. He coined and pioneered the field of piezotronics and piezo-phototronics by introducing piezoelectric potential gated charge transport process in fabricating new electronic and optoelectronic devices. Details can be found at: www.nanoscience.gatech.edu.

**Xia Cao** is currently a distinguished professor at the University of Science and Technology Beijing, and a professor at the Beijing Institute of Nanoenergy and Nanosystems, Chinese Academy of Sciences. Her main research interests include energy materials, nanogenerator, energy conversion and storage, flexible electronic sensor, and self-powered system.

**Liqun Zhang** is a professor of Beijing University of Chemical Technology. His research interests focus on rubber science and technology, polymer nanocomposites, bio-based polymeric materials and so on. He has received various famous awards such as National Outstanding Youth Foundation, Changjiang Scholar Professor of Ministry of Education of China, Sparks-Thomas sci-tech award of Rubber Division of American Chemical Society, Science of Chemical Engineering of Japan (SCEJ) Research award, and Morand Lambla Award of International Polymer Processing Society. He has published over 300 peer-reviewed papers, and has given over 60 plenary/ keynote/invited lectures in international conferences.